

Article

Extremal Analysis of Flooding Risk and Its Catastrophe Bond Pricing

Jiayi Li ¹, Zhiyan Cai ², Yixuan Liu ³ and Chengxiu Ling ^{4,*}¹ Department of Science Statistics with Data Science, The University of Edinburgh, Edinburgh EH15 1LR, UK² Institute of Health Informatics, University College London, London WC1H 9BT, UK³ Department of Financial and Actuarial Mathematics, Xi'an Jiaotong-Liverpool University, Suzhou 215123, China⁴ Academy of Pharmacy, Xi'an Jiaotong-Liverpool University, Suzhou 215123, China

* Correspondence: chengxiu.ling@xjtlu.edu.cn; Tel.: +86-512-8188-9023

Abstract: Catastrophic losses induced by natural disasters are receiving growing attention because of the severe increases in their magnitude and frequency. We first investigated the extreme tail behavior of flood-caused economic losses and maximum point precipitation based on the peaks-over-threshold method and point process (PP) model and its extreme tail dependence. We found that both maximum point precipitation and direct economic losses are well-modeled by the PP approach with certain tail dependence. These findings were further utilized to design a layered compensation insurance scheme using estimated value-at-risk (VaR) and conditional VaR (CVaR) among all stakeholders. To diversify the higher level of losses due to extreme precipitation, we designed a coupon paying catastrophe bond triggered by hierarchical maximum point precipitation level, based on the mild assumption on the independence between flood-caused risk and financial risk. The pricing sensitivity was quantitatively analyzed in terms of the tail risk of the flood disaster and the distortion magnitude and the market risk in Wang's transform. Our trigger process was carefully designed using a compound Poisson process, modeling both the frequency and the layered intensity of flood disasters. Lastly, regulations and practical suggestions are provided regarding the flood risk prevention and warning.

Keywords: extreme value theory; peaks-over-threshold; CAT bond; point process; Vasicek model; tail dependence; distortion measure; floods

MSC: 91B30; 62P12; 60G55; 91B05; 91G70; 62G32; 60G70; 91G15; 91G30; 91G60; 97M30; 62P05



Citation: Li, J.; Cai, Z.; Liu, Y.; Ling, C. Extremal Analysis of Flooding Risk and Its Catastrophe Bond Pricing. *Mathematics* **2023**, *11*, 114. <https://doi.org/10.3390/math11010114>

Academic Editors: Zhengjun Zhang, Yanxi Hou and Leonid V. Bogachev

Received: 23 September 2022

Revised: 23 November 2022

Accepted: 26 November 2022

Published: 27 December 2022



Copyright: © 2022 by the authors. Licensee MDPI, Basel, Switzerland. This article is an open access article distributed under the terms and conditions of the Creative Commons Attribution (CC BY) license (<https://creativecommons.org/licenses/by/4.0/>).

1. Introduction

Extreme weather events threaten human lives and cause huge financial losses. Under the changing climate conditions, natural disasters might simultaneously occur, placing a heavy burden on the healthcare system and necessitating economic reconstruction [1]. In the Asian monsoon season, the rain usually triggers floods, especially in the basin of the largest river in China [2,3]. The historic large floods in China have caused over RMB 200 billion in losses per decade. The latest one occurred in 2021, in Zhengzhou, China, during which 457.5 mm of precipitation fell within 24 h and caused severe flooding, and resulting in RMB 53.2 billion in economic losses and more than RMB 6.4 billion in insurance claims caused by damage to more than 4×10^5 cars. Such severe disasters occur frequently all over the world [2]. Despite the many advances in science and technology regarding transferring disaster risks, extreme weather still causes great losses. To establish risk warning systems and risk diversification, it is crucial to accurately model such extreme risks because unexpected disaster risks might cause breakdowns of healthcare systems due to insufficient risk warning systems.

In this study, our aim was discover the extreme dependence between the severity of floods and their direct economic losses in the framework of extreme value theory, which is

widely applied in financial and environmental fields, see, e.g., [4–8] for application in the study of financial crises, the super-spreading of COVID-19, and severe rainstorms. This is implemented in two stages: the study of marginal tail performance and the investigation of the extreme comovement through typical bivariate models. The former is conducted through the univariate extreme value theory with the competitive point process approach for the threshold excesses, compared with the peaks-over-threshold based generalized Pareto models in [9]. The tail analysis of floods can assist in furthering the quantitative analyses of risk measures and risk vulnerability ranking [10]. The tail dependence is measured by both the upper tail dependence coefficient (UTDC) and tail quotient correlation coefficient (TQCC), which confirmed the comovement of extreme precipitation and economic losses, see, e.g., [11,12] for the study of UTDC and TQCC.

As an application of the extreme tail behavior of maximum point precipitation and direct economic losses in Section 2, we designed a layered compensation insurance scheme following the workflow in Figure 1 according to the estimated value-at-risk (VaR) and conditional VaR (CVaR) in Table 3. Essentially, we extrapolated the tail behavior of the generalized Pareto distributed economic losses to obtain the estimates of VaR and CVaR at three extreme risk levels of $\alpha = 90\%, 95\%$, and 97.5% . The pricing mechanism of a flooding catastrophe bond is described in Section 3 using homogeneous compound Poisson processes. Given climate changes and financial volatility as well as economic uncertainty [1,9,13,14], the sensitivity of this CAT bond was analyzed via the tail index (shape parameter) of precipitation and financial market distortion, shown in Figure 6. We provide policy makers in Section 4 with constructive suggestions for allocating abundant monetary support and flood risk prevention among investors, reinsurers, and insurers.

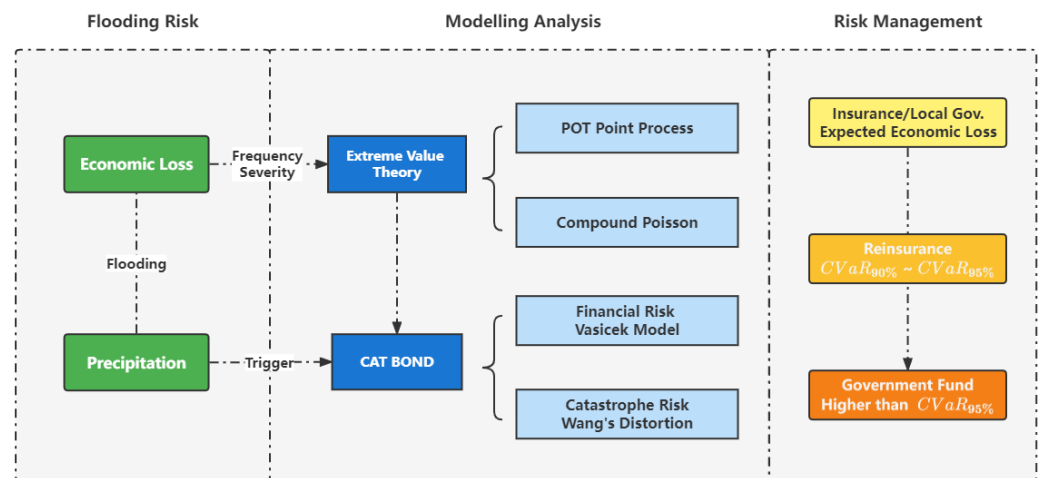


Figure 1. Workflow of flooding risk management.

The remainder of this paper is organized as follows. Section 2 shows the extreme features of maximum point precipitation and the resulting flooding economic losses. Section 3 provides the main results and is followed by Section 4, which outlines our conclusions. We end this paper with Appendices A and B describing all methodologies involved.

2. Data Preprocessing of Flooding Economic Losses and Precipitations

In order to study the catastrophe losses caused by flooding in various regions in China, we collected 369 recorded provincial direct economic losses (DELs) of main flooding events distributed throughout 31 major provinces in China from 2004 to 2019 from <http://www.mwr.gov.cn/sj/> accessed on 1 January 2020, the official website of the Ministry of Water Resources of the People’s Republic of China. Accordingly, 99 maximum point precipitation values (the maximum accumulated precipitation in a particular site within exactly 24 h) were recorded for the main rainstorms because most provincial DELs were recorded along with the alternative precipitation indices, e.g., cumulative precipitation

or average precipitation. Only major events were considered as the events with minor effects were already filtered by the officials. Therefore, in the following, all risk analysis was performed based on the data available from 2004 to 2019 after being adjusted based on the consumer price index (CPI) of 2019.

We see from Table 1 that the average economic loss produced by the main flooding events in China from 2004 to 2019 was RMB 2.47 billion, with a large range from RMB 0.004 billion to 54.324 billion. Figure 2 shows that both direct economic loss and maximum point precipitation seem roughly right skewed with a certain positive association for the bulk of the data. Precipitation, one of the major drivers of floods that might concur with typhoons and rainstorms, is not affected by humans. This, together with the marginal tail behavior and the tail dependence, motivated our trigger design of precipitation level for the catastrophe bond in Section 3.2. In particular, the 85%, 90%, 95%, and 99% quantile precipitations were 803.4, 844, 970.89, and 1247.25, respectively.

Table 1. Descriptive analysis of direct economic loss (DEL) in billion yuan and maximum point precipitation (MPP) in millimeters.

Variable	Size	Min	Median	Mean	Max	Skewness	Kurtosis
DEL	369	0.004	0.795	2.47	54.324	5.45	41.79
MPP	99	75	476	525.27	1426	0.79	3.63

Source: <http://www.mwr.gov.cn/sj/> (accessed on 1 January 2020), the Ministry of Water Resources of China.

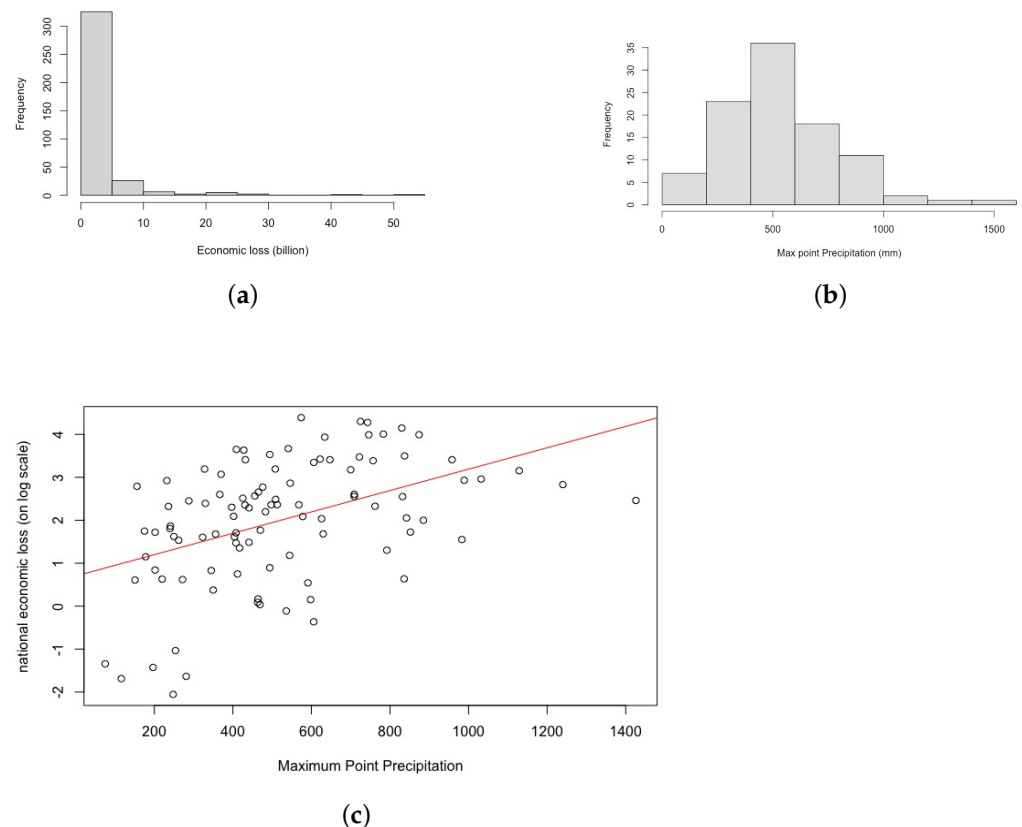


Figure 2. Histogram of (a) economic loss and (b) maximum point precipitation, and (c) scatter plot of economic loss in billion yuan on log scale against maximum point precipitation in millimeters.

In summary, the economic loss caused by severe floods is highly associated with extreme precipitation. We established extreme models to conduct flooding risk management through insurance and reinsurance companies as well as financial markets.

3. Main Results

In risk management, of importance is designing a layered compensation system among all stakeholders and thus diversify potential risk in insurance, reinsurance, and financial markets. This section presents our main results from analyzing the extreme behavior of flooding economic losses and precipitation in Section 3.1, and the latter was applied to determine the natural disaster risk in the pricing of flooding catastrophe bonds, as described in Section 3.2.

3.1. Extreme Analysis of Flooding Economic Losses and Precipitations

We applied extreme value theory (EVT) to analyze the tail distribution law of the economic loss caused by severe floods. Given the limited datasets, we considered the compound Poisson process of excess loss specified below. Let $S_{N(t)}$ be the total excess loss since 2004, given by

$$S_{N(t)} = \sum_{i=1}^{N(t)} X_{iu}, \quad t \geq 0,$$

where X_{iu} is the i th excess loss over a proper threshold u in the following t years, and $N(t)$, $t \geq 0$ denotes the number of excess losses caused by severe floods in the following t years. The independence between the frequency of excess loss $N(t)$ and excess loss X_{iu} is acceptable according to Fisher’s exact test with $p = 0.2597$. Thus, the expected total excess loss is obtained by

$$\mathbb{E}\{S_{N(t)}\} = \mathbb{E}\{N(t)\}\mathbb{E}\{X_u\}. \tag{1}$$

In this study, the economic loss threshold u , which helps to identify the GP-distributed excess losses $X_u := (X - u)|X > u$, was set to 1.879, following the rule of thumb proposed by [15], i.e., the threshold was selected to ensure the number of exceedances $k = n^{2/3} / \log(\log n)$ out of n observations, adjusted by the graphical diagnosis in Figure 3, namely, the mean residual and threshold stability plots [16,17]. The linear pattern of the sample mean excess probably indicates a power-decaying tail behavior of large economic losses. The result of the Kolmogorov–Smirnov test of the GP-distributed excess showed $p = 0.8422$, confirming its appropriateness.

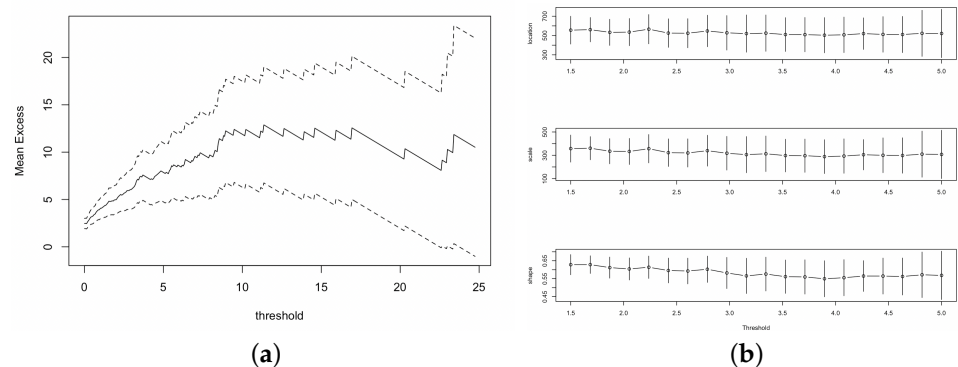


Figure 3. (a) Sample mean excess for economic loss in billion yuan with grey dash line representing 95% confidence interval. (b) Variation plots of location, scale, and shape (from top to bottom) against threshold $u \in (1.5, 5)$.

To discern the power tail feature from the double exponential behavior (i.e., $\zeta = 0$ for the exponential decay tail of the threshold excess) and the short tail (i.e., $\zeta < 0$ using the generalized Pareto model (GP)), we apply the excess models given in Appendix A. Namely, we fit the excess losses by the point process, and compared the result with that of the GP and exponential models (i.e., the reduced model of GP with $\zeta = 0$). The obtained estimates of the parameters are shown in Table 2. We see that the point process model was the best, having a minimum AIC and BIC when fitting the excess losses, and the power

tail feature was confirmed by both GP and PP models because the 95% confidence interval extended well above zero. We obtained the maximum-likelihood estimate of the location, scale, and shape parameters as $(\hat{\mu}, \hat{\sigma}, \hat{\zeta}) = (57.33, 34.02, 0.57)$, respectively, by maximizing Equation (A6).

Table 2. AIC, BIC, and estimates of the location, scale, and shape parameters with standard errors (s.e.) in parentheses when fitting economic excess losses by point-process (PP), generalized Pareto (GP), and exponential (Exp.) models. Here, the threshold $u = 1.879$.

Model	Location Parameter (μ)		Scale Parameter (σ)		Shape Parameter (ζ)		AIC	BIC
	Estimates (s.e.)	95% CI	Estimate (s.e.)	95% CI	Estimate (s.e.)	95% CI		
PP	57.33 (15.60)	(26.76, 87.91)	34.02 (13.82)	(6.92, 61.11)	0.57 (0.10)	(0.38, 0.77)	-273.544	-265.416
GP	-	-	2.30 (0.41)	(1.49, 3.11)	0.61 (0.16)	(0.29, 0.93)	545.641	551.060
Exp	-	-	4.91 (0.47)	(3.99, 5.82)	-	-	577.059	579.769

To determine the expected total annual excess loss, it remained to check if the frequency of excess loss followed Poisson distribution. We employed the KS test and obtained a p -value equal to 0.7132, which suggested the annual frequency of excess economic loss followed a Poisson distribution with an annual mean $\hat{\lambda} = 6.94$. Consequently, the total annual excess economic loss was estimated as $\text{RMB } 6.94 \times 5.89 = 38.94$ billion using Equations (1) and (A4).

Note that VaR and CVaR are two common risk measures applied to evaluate extreme risks with good mathematical properties and are practically meaningful in the insurance and finance fields. Applying the extrapolation approach (c.f. Equations (A3) and (A5)), Table 3 shows the estimates of VaR and CVaR at different confidence levels, formalizing the compensation system.

In particular, we specified three loss levels for the compensation mechanism using the VaR and CVaR values, which could be covered among all stakeholders, including the local government, reinsurers, and government funds such as catastrophe bonds. For higher loss levels, insurance companies may generally transfer the higher risk to reinsurers as well as the financial markets in terms of various financial securities [3]. Thus, in Section 3.2, we describe the price of a flooding catastrophe bond.

Table 3. Design of compensation mechanism according to VaR and CVaR of individual economic loss.

Confidence Level	VaR	CVaR	Loss Level	Loss Amount (Billion RMB)	Loss Taker
97.5%	13.37	34.22	Third level	>22.28	Government (CAT bond)
95.0%	8.24	22.28	Second level	14.24–22.28	Re-insurance
90.0%	4.78	14.24	First level	4.78–14.24	CRFCIF ¹

¹ Cross-Regional Flooding Catastrophe Insurance Fund.

3.2. Design of Flooding Catastrophic Bonds

Trigger selection is of prime importance in the design of CAT bonds. In general, indemnity and nonindemnity triggers constitute the trigger classification. The bases of how they are triggered are the sponsor’s actual loss caused in specified catastrophic occurrences and other quantities for reflecting or approaching the actual loss, e.g., 2015 Acorn Re earthquake CAT bond. This bond was also adopted as the guide for our analysis of the CAT bond triggered by large maximum point precipitation levels. To reconfirm that the maximum point precipitation was a proper trigger choice, we adopted upper tail dependence coefficient (UTDC) and tail quotient correlation coefficient (TQCC) between the maximum point precipitation and economic loss to assist in our discussion. In our calculations, the assumption of the identical and independent distributions of the maximum point precipitation X_i (direct economic losses Y_i) was confirmed by a Ljung–Box test with a

p -value of 0.8177 (0.2829). Therefore, the subsequent empirical tail dependence analyses could then be conducted. The empirical u -level tail dependence index is represented as:

$$\chi_n(u) := 1 - \frac{\log \mathbb{P}\{F_{n1}(X_i) < u, F_{n2}(Y_i) < u\}}{\log u},$$

where F_{n1} and F_{n2} are the empirical marginal distributions of (X_i, Y_i) . We see from Figure 4a that $\chi_n(u)$ remains constant for a moderate quantile level. This indicates that large economic losses are likely to occur along with large maximum point precipitation. The tail dependence index χ , as the limit of $\chi(u)$, was estimated as $2 - 2^{0.6734} = 0.405$, applying a bivariate logistic model for the 90% quantile excess [11]. Meanwhile, we analyzed the relative extremes of the corresponding threshold exceedances with the tail quotient correlation coefficient (TQCC), see, e.g., [12]. Namely,

$$q(u) = \frac{\max_{1 \leq i \leq m} \left(\frac{\max(\tilde{X}_i, t_u)}{\max(Y_i, t_u)} - 1 \right) + \max_{1 \leq i \leq m} \left(\frac{\max(\tilde{Y}_i, t_u)}{\max(\tilde{X}_i, t_u)} - 1 \right)}{\max_{1 \leq i \leq m} \frac{\max(\tilde{X}_i, t_u)}{\max(Y_i, t_u)} \times \max_{1 \leq i \leq m} \frac{\max(\tilde{Y}_i, t_u)}{\max(\tilde{X}_i, t_u)} - 1}, \quad t_u = -1/\log u, \quad u \in (0, 1),$$

where $(\tilde{X}_i, \tilde{Y}_i)$ is the unit Fréchet distributed threshold exceedances based on the marginal analysis in Section 2, i.e.,

$$\tilde{X}_i = - \left(\log \left\{ 1 - \zeta_X \left[1 + \hat{\zeta}_X \frac{X_i - u_X}{\hat{\sigma}_X} \right]^{-1/\hat{\zeta}_X} \right\} \right)^{-1}, \quad \tilde{Y}_i = - \left(\log \left\{ 1 - \zeta_Y \left[1 + \hat{\zeta}_Y \frac{Y_i - u_Y}{\hat{\sigma}_Y} \right]^{-1/\hat{\zeta}_Y} \right\} \right)^{-1},$$

where $\zeta_X = 1 - F_X(u_X)$ and $\zeta_Y = 1 - F_Y(u_Y)$. We see from Figure 4b that TQCC shows an increasing trend with values apparently larger than 0.1. Therefore, large maximum point precipitation may indicate large economic losses [18]. The naturally arising question for insurers and reinsurers is how to hedge large risk.

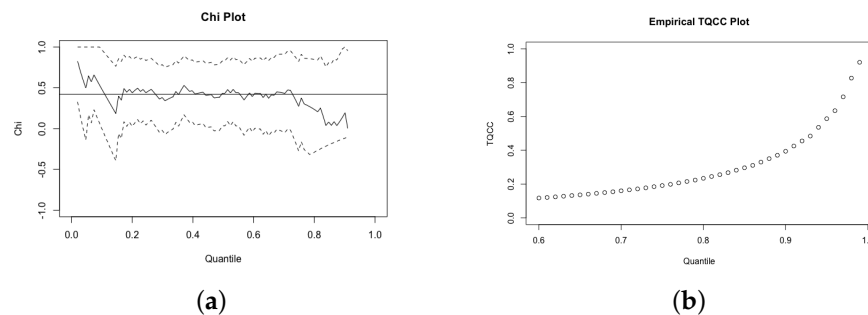


Figure 4. The empirical tail dependence measures (a) the Chi plot $\chi_n(u)$ and (b) the tail quotient correlation coefficient $q(u)$. The solid lines and dotted lines show the estimate and 95% pointwise confidence intervals, respectively. The estimate of the tail dependence index $\hat{\chi} = 2 - 2^{0.6734} = 0.405$ is indicated by the horizontal line using the bivariate logistic extreme value model.

The bond market is a logical choice because investors are looking for arbitrage opportunities and can mitigate the loss of insurance products. Collateralized special purpose vehicles (SPVs) issue the CAT bond, which is usually issued and established by sponsors who are insurers and reinsurers. For SPVs, the premium is paid by the sponsor, and reinsurance is used as a return. The incentive premium is usually paid to investors as part of the coupon payment, including the oscillation part related to the national reference interest rate. For example, the London Interbank Offered Rate (LIBOR) and Shanghai Inter-bank Offered Rate (Shibor) can reflect the return from the trust account where the principal is deposited. The principal and coupon payments are reduced whenever a specific triggering event happens. Additionally, sponsors can receive some funds as a repayment for the claims. Here, we followed the product pricing scheme proposed by [3], together with a

compound Poisson trigger process similar to the 2015 Acorn Re earthquake CAT bond. The detailed workflow is presented in Figure 5.

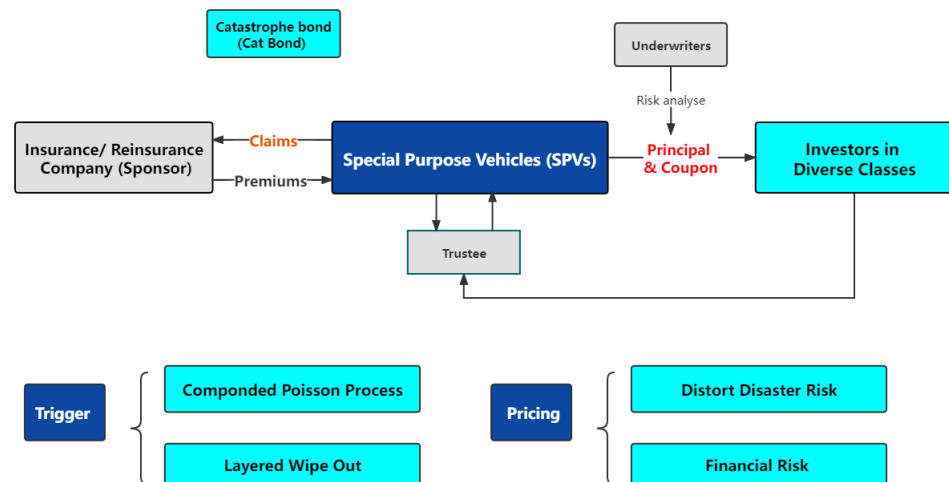


Figure 5. Operation mechanism for catastrophe bonds.

Here, we considered a payoff function $\Pi(\cdot)$ and wiped out time τ defined by

$$\Pi(y) = \max\{1 - y, 0\}, \quad y \geq 0, \quad \tau = \inf\{t \geq 0 : \Pi(Y_t) = 0\}.$$

Here, the trigger process $\{Y_t, t \geq 0\}$ was supposed as a compound Poisson trigger process given as

$$Y_t = \sum_{j=1}^{N_t} (0.005 \times \mathbb{I}(X_j \in (803.4, 844]) + 0.01 \times \mathbb{I}(X_j \in (844, 970.89]) + 0.015 \times \mathbb{I}(X_j \in (970.89, 1247.25]) + 0.05 \times \mathbb{I}(X_j \in (1247.25, \infty))),$$

where X_j denotes the severity of the flooding driver (here, maximum point precipitation), and N_t denotes the number of large maximum point precipitation events up to time t . The four maximum point precipitation levels of 803.4, 844, 970.89, and 1247.25 accounts for the 0.85, 0.9, 0.95, and 0.99 quantiles, respectively, which means when severity is above a certain level of threshold, a fraction 0.5%, 1%, 1.5%, 5% of the principal will be wiped off.

For example, we issue a bond with a face value of 1000 (denoted by K), a maturity of 3 (denoted by T), and a coupon period of 1/4 year (denoted by Δ). The bonds will be paid at $s\Delta$, where $s = 1, \dots, 4T$. It follows from Equation (A8) that the price at time t becomes

$$P_t = \frac{K}{4} \mathbb{E}^{Q^1} \left[\sum_{s=\lfloor t \rfloor + 1}^{\lfloor 4\tau \rfloor \wedge 4T} \mathbb{E}^{Q^2} \left[D(t, s\Delta)(R + i_{s\Delta})\Pi(Y_{(s-1)\Delta}) \right] \right] + KQ^1(\tau > T) \mathbb{E}^{Q^2} [D(t, T)\Pi(Y_T)] + \frac{K}{4} \mathbb{E}^{Q^1} \left[(\tau - \lfloor \tau \rfloor \Delta) \mathbb{I}(\tau \leq T) \Pi(Y_{\lfloor \tau \rfloor}) \mathbb{E}^{Q^2} [D(t, \tau)(R + i_\tau) \mid \tau] \right]. \tag{2}$$

Note that the pricing scheme can only be realized by Monte Carlo simulation. To achieve this, we modeled the maximum point precipitation excess by generalized Pareto distribution $GP_{\xi, \beta}$ following a similar procedure to that used for direct economic losses in Section 3. All the estimates of parameters involved were given in Table 4. We modeled the annual number of maximum point precipitation excess events as a Poisson distribution and obtained an intensity λ of 6.94. Furthermore, we implemented Wang’s distortion of disaster risk X [19], i.e.,

$$\tilde{X} = \left[(1 - \Phi(\Phi^{-1}(U) + \kappa))^{-\xi} - 1 \right] \times \frac{\beta}{\xi} + u.$$

Additionally, the financial interest risk (r_t, ℓ_t) in Equation (A9) was fitted by the 4 years and 3 months China treasury bond rates and 4 years and 3 months Shanghai inter-bank offered rate (Shibor). Estimated parameters were put into the pricing measure that combined a distorted pricing measure representing catastrophe insurance risk and a risk-neutral pricing measure for the arbitrage financial market. The bond price was given by a simulation of 10^5 paths, each with distorted generalized Pareto distributed interarrival time.

Table 4. Parameters of interest rate and precipitation modeling.

Panel A: Vasicek models (under Q^2)								
Risk-free rate				Shibor			Correlation	
a_r	b_r	σ_r	r_0	a_ℓ	b_ℓ	σ_ℓ	ℓ_0	ρ
1.52	4.12%	1.40%	2.28%	0.04	2.02%	4.00%	2.43%	0.89
Panel B: Maximum point precipitation distribution								
Under \mathbb{P}^1				Under Q^1				
$\mathbb{P}\{X > u\} = 10\%$ $X - u (X > u) \sim GP_{\xi, \beta}$ $\xi = -0.0558, \beta = 186.6225$ $u = 844$ Maximum magnitude: 4187				$Q^1(X \leq x) = \Phi(\Phi^{-1}(P^1(X \leq x)) - \kappa)$ $\kappa = 1.24$				

Figure 6a shows the price variations in the financial market risk in terms of the distortion parameter $\kappa \in (0, 1.5)$ of Wang’s transform. A larger value of κ means that investors are exposed to higher risk, so a higher premium will be required, as well as, eventually, a lower bond price. In addition, the practical value of $\kappa = 1.24$ was determined when we set the par value $K = 1000$ to be equal to the bond price. Furthermore, the sensitivity analysis was conducted for its shape parameter, presented in Figure 6b. At this time, the ratio of scale (β) to shape (ξ) was -3342.863 , which means the maximum (the right endpoint) keeps unchanged at 4186.863. We found that the bond price increased with decreasing shape parameter, which is reasonable in reality as investors are exposed to higher risk and require lower costs/higher returns at this time.

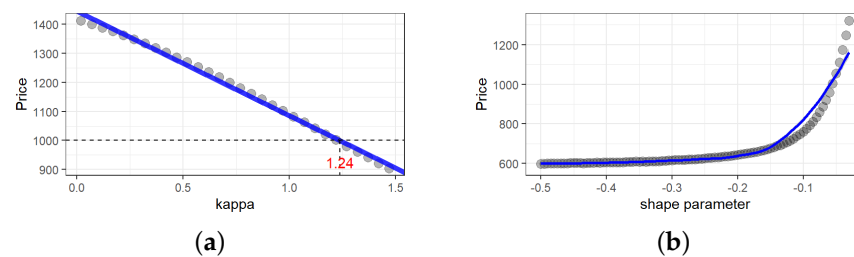


Figure 6. The empirical price at $t = 0$ varies with (a) the distortion parameter κ and (b) the shape parameter ξ with $\beta/\xi = -3342$, $\kappa = 1.24$. Here, the empirical price is given by Equation (2) and a simulation of 10^5 samples of the threshold excess of maximum point precipitation from $GP_{\xi, \beta}$, with all other parameters specified in Table 4.

4. Conclusions and Extension Discussions

We determined the marginal tail behaviors of maximum point precipitation events reflecting both the severity of floods in a 24 h rainstorm and its resulting vulnerability risk via the direct economic losses. These findings suggest a compensation mechanism among local, state, and national governments as well as financial markets. Market regulators and investors can utilize our findings for pricing flooding CAT bonds to either mitigate the risk or gain arbitrage according to their real information, e.g., past economic loss, catastrophe frequency, magnitude, and past interest rate. Moreover, they can adjust the price according to their risk attitude or risk tolerance. For instance, pessimistic investors tend to increase the distortion parameter κ and increase the absolute value of the shape parameter to mitigate their risk. Otherwise, they may lower these parameters to be actively involved in this

market to gain arbitrage. When a market regulator is highly optimistic about the decrease in severity and frequency of a catastrophic event, then the distortion parameter and absolute value of the shape parameter could be lowered and vice versa. Moreover, this pricing framework and implementation of EVT can be adapted to various kinds of catastrophe events including hurricanes, earthquakes, and typhoons [20].

This study lays a foundation for further studies on compound disaster modeling and systemic risk management strategy. In practice, multiple disasters may simultaneously occur or in a chain, e.g., wildfire and air pollution and morbidity from lung-related diseases [21]. Additionally, the regional vulnerability to different natural disasters might be further considered in the future provided that spatial–temporal hydrology data with high enough is available, see, e.g., [22,23] for related studies on spatial modeling of extreme precipitations and grey relational analysis. Given that fine pixel data are available on certain spatial and temporal scales, alternative models of the occurrences of disasters may be applied, including log-Gaussian Cox processes [24] and nonhomogeneous compound Poisson process of the total excess economic losses involved, possibly explained by growing climate change, seasonal clustering factors, as well as different weather types [9]. Finally, the single-trigger CAT bond in this study lays the foundation for multiple-event trigger CAT bonds using the Copula–EVT framework and multiple financial risks including inflation risk (i.e., randomized CPI) and interest risks reflecting economic uncertainty as well [13,25,26].

Author Contributions: Conceptualization, C.L. and Y.L.; methodology, Z.C.; software, J.L.; validation, J.L. and Z.C.; formal analysis, Y.L.; investigation, Z.C. and J.L.; resources, Y.L.; data curation, Y.L.; writing—original draft preparation, J.L. and Z.C.; writing—review and editing, C.L. and J.L.; visualization, Y.L.; supervision, C.L.; project administration, C.L.; funding acquisition, C.L. All authors have read and agreed to the published version of the manuscript.

Funding: This study was funded by the Research Development Fund at XJTLU (RDF1912017) and the Post-graduate Research Scholarship (PGRS2112022) and Jiangsu Qinglan Talent in 2022.

Institutional Review Board Statement: Not applicable.

Informed Consent Statement: Not applicable.

Data Availability Statement: The data are available from <http://www.mwr.gov.cn/sj/>.

Acknowledgments: We thank the editors and all reviewers for their constructive suggestions and comments that greatly helped to improve the quality of this paper. The authors would also thank Yifan Tang for the data cleaning.

Conflicts of Interest: The authors declare no conflict of interest.

Appendix A. Extreme Value Theory

Extreme value theory is a natural tool used to model severe floods and their resulting huge economic loss because a few extreme precipitation events result in more than 90% of the annual economic losses. Flood risk management institutions should focus on the maxima and tail exposures instead of the expected average outcome of compartmental models.

Block maxima (BM) and peaks-over-threshold (POT) are two common approaches used for extracting extreme data, which can be fitted by generalized extreme distribution (GEV) and generalized Pareto distribution under certain conditions, respectively [4,27]. Both methods face a common challenge in overcoming model uncertainty. Both can be interpreted in terms of Poisson point processes with certain relationships of the parameters involved. Given a high threshold u , suppose that the threshold excess of X is well fitted by a generalized Pareto (GP) distribution $GP(y; \tilde{\sigma}, \tilde{\zeta})$. Then, the exceedance probability of X over larger x can be represented as (note $\bar{F}(u) = 1 - F(u)$)

$$1 - F(x) = \bar{F}(u)\mathbb{P}\{X > x | X > u\} \approx \bar{F}(u)GP(x - u; \tilde{\sigma}, \tilde{\zeta}), \quad x > u. \quad (\text{A1})$$

Here, u is a proper threshold so that an amount of excesses $(x_i - u)$ of n samples asymptotically follows GP distribution, which further leads to a maximum likelihood estimate of ξ and $\tilde{\sigma}(u) = \sigma + \xi(u - \mu)$. The triple (μ, σ, ξ) consists of the location, scale, and shape parameters involved in the GEV model, which fits the block maxima M_n of an independent and identically distributed sample X_1, \dots, X_n from parent $X \sim F$, i.e.,

$$\mathbb{P}\{M_n \leq x\} \approx G(x; \mu, \sigma, \xi) := \exp\left(-\left(1 + \xi \frac{x - \mu}{\sigma}\right)_+^{-1/\xi}\right). \tag{A2}$$

The exceedance probability in Equation (A1) provides the information on the amount of time that a risk is expected to exceed certain performance levels, which is commonly used to predict extreme events such as floods, hurricanes, and earthquakes. In addition, we may invert Equation (A1) to obtain a high quantile of the underlying distribution or the T -year return level stated below.

For $T > 1/\bar{F}(u)$, we have the T -year return level (i.e., the average time of x_T has been exceeded per T observations, with exceeding probability $p = 1/T$), defined as,

$$x_T = u + \frac{\tilde{\sigma}}{\xi} \left(\left(\frac{1}{T\bar{F}(u)} \right)^{-\xi} - 1 \right).$$

Thus, the minimum level that a potential risk X is exceeded with small probability $1 - q$, the so-called value-at-risk (VaR) at level q , denoted by $\text{VaR}_q(X)$, is given by

$$\text{VaR}_q(X) = u + \frac{\tilde{\sigma}}{\xi} \left(\left(\frac{1 - q}{\bar{F}(u)} \right)^{-\xi} - 1 \right), \quad q > F(u). \tag{A3}$$

VaR is commonly used as a risk measure to determine the potential capital premium due to its simplicity and back-testing properties. However, it neither reflect the tail magnitude nor satisfy subadditivity in general. Alternatively, conditional value-at-risk (CVaR), which is defined as the expected value of the exceedance of the VaR, is the unique coherent, and back-testing risk measure. We have

$$\text{CVaR}_p(X) = \mathbb{E}\{X|X > \text{VaR}_p(X)\} = \text{VaR}_p(X) + \mathbb{E}\{X - \text{VaR}_p(X)|X > \text{VaR}_p(X)\}.$$

Note that CVaR is also called the expected shortfall, giving insight into the magnitude of an extreme loss. Therefore, the bank and insurer may prefer CVaR to VaR in the process of policy making. Both are widely used in optimal allocations of resources and assets, see, e.g., [28].

Because the threshold excesses follow an asymptotically generalized Pareto distribution, we may approximate the tail expectations as

$$\mathbb{E}\{X - u|X > u\} \approx \frac{\tilde{\sigma}(u)}{1 - \xi} = \frac{\sigma + \xi(u - \mu)}{1 - \xi}, \quad \xi < 1. \tag{A4}$$

Thus,

$$\text{CVaR}_p(X) = \text{VaR}_p(X) + \frac{\tilde{\sigma}(\text{VaR}_p(X))}{1 - \xi} = \frac{\text{VaR}_p(X)}{1 - \xi} + \frac{\sigma - \xi\mu}{1 - \xi}. \tag{A5}$$

We can obtain estimates of exceedance probability, VaR, and CVaR defined in Equations (A1), (A3) and (A5), respectively, with related parameters estimated and empirical survival probability $\hat{F}(u) = n_u/n$ provided that n_u exceedances over u come from a sample of size n .

In addition to the aforementioned GEV and GP models, the block maxima, and threshold excesses, a particularly elegant formulation of characterizing the extreme value

behavior is derived from the theory of point processes (PP), which considers exceedances of the threshold as events in time and models thus both the occurrence and intensity of exceedances. Given a sequence of r.v. X_i with values in a state space \mathcal{A} , we define, for any set $A \subset \mathcal{A}$, the r.v. $N(A)$ denotes the number of X_i value in the subset A that can formalize a point process under certain conditions. The intensity measure of this process is one of the key summary features, defined as

$$\Lambda(A) = \mathbb{E}\{N(A)\}.$$

This returns the expected number of values in the corresponding subset A . The intensity density function is then defined by its derivative function if this exists with $A = \prod_{i=1}^d [a_i, x_i]$, i.e.,

$$\lambda(x) = \frac{\partial \Lambda(A)}{\partial x_1 \cdots \partial x_d}.$$

For a homogeneous Poisson point process, the parameter λ is a positive constant, such that for $A = [t, s] \in T$,

$$N(A) \sim \text{Poisson}(\lambda(s - t)).$$

Let X_1, \dots, X_n be an independent and identically distributed sequence, which may consist of the observation of a potential risk X satisfying Equation (A1) or (A2). Then, the point process of $(i/(n + 1), X_i)$ on $A = [t_1, t_2] \times (u, \infty) \subset [0, 1] \times \mathbb{R}$, denoted by $N(A)$, is given as

$$N(A) := \#\{i \in \mathbb{N}, t_1 \leq i/(n + 1) \leq t_2, X_i > u\}, \quad A = [t_1, t_2] \times (u, \infty).$$

Under some weak conditions, we have $N(A) \sim \text{Poisson}(\Lambda(A))$ holds asymptotically with intensity measures given below:

$$\Lambda(A) = \int_{(t,x) \in A} \lambda(t, x) dt dx = (t_2 - t_1) \cdot \left[1 + \xi \frac{u - \mu}{\sigma} \right]^{-\frac{1}{\xi}} \cdot \mathbb{I}(1 + \xi \cdot (u - \mu)/\sigma > 0),$$

where $\xi, \mu \in \mathbb{R}$, and $\sigma > 0$ represent the shape, location, and scale parameters, respectively. $\mathbb{I}(\cdot)$ is the indicator function, see Theorem 7.1.1 in [16]. Maximum likelihood estimation was adopted here to estimate the parameters involved in the PP model. PP log-likelihood, $\ell(\cdot)$, for a high threshold u , is given as

$$\begin{aligned} &\ell(\mu, \sigma, \xi; x_1, \dots, x_n) \\ &= -n_u \ln \sigma - \left(\frac{1}{\xi} + 1\right) \sum_{i=1}^n \ln \left(1 + \frac{\xi}{\sigma} (x_i - \mu)\right) \mathbb{I}(x_i > u) - \left(1 + \frac{\xi}{\sigma} (u - \mu)\right)^{-\frac{1}{\xi}}. \end{aligned} \tag{A6}$$

Though this log-likelihood function considers excesses, the parameterization is based on the GEV distribution function, and thus is invariant to the threshold. Consequently, the PP model can be adapted to allow for nonstationary effects to include temporal or covariates' effects in the parameters even with time-varying thresholds [27].

Appendix B. A Pricing Scheme of Catastrophe Bonds

The trigger model, payoff function, principal wipe-out function, and accrued coupon should be determined prior to pricing measurement because coupon payment and principal redemption might be changed once a catastrophe (CAT) event occurs.

Consider a trigger process $\{Y_t, t \geq 0\}$ as a component-wise nondecreasing, non-negative, and right continuous stochastic process:

$$Y_t = f(X_1, X_2, \dots, X_{N_t}), \quad t \geq 0, \tag{A7}$$

where $\{X_n, n \in \mathbb{N}\}$ is a sequence of random variables modeling precipitation severity, and $\{N_t, t \geq 0\}$ is a counting process to model the occurrence of floods, and f is a component-wise nondecreasing function.

There are various kinds of triggers Y , for instance:

- (i) The aggregate amount of loss due to natural disasters, e.g., floods;
- (ii) The number of large floods, which considers both magnitude and frequency as below

$$Y_t = \sum_{j=1}^{N_t} \mathbb{I}(X_j > u), \quad u \geq 0,$$

where u is a high threshold and $N(t)$ is the number of exceedances over the threshold observed in $[0, t]$.

Next, the pay-off function $\Pi(y) : [0, \infty) \mapsto [0, 1]$ is a nonincreasing function linking the natural disaster risks via the trigger process $Y_t = f(X_1, \dots, X_{N(t)})$ and the financial securities. Especially, the time of principal being wiped out is denoted by

$$\tau = \inf\{t \geq 0 : \Pi(Y_t) = 0\}.$$

Next, we introduce the pricing measure as a product of the natural disaster risk and financial risk. The pricing at time t is essentially the discounted value of future coupon payments plus the discounted value of the remaining principal.

$$\begin{aligned} P_t &= K\mathbb{E}_t^{Q^1 \times Q^2} \left[\sum_{s=[t]+1}^{\lfloor \tau \rfloor \wedge T} D(t, s)(R + i_s)\Pi(Y_{s-1}) + D(t, \tau)\mathbb{1}(\tau \leq T) + D(t, T)\Pi(Y_{s-1}) \right] \\ &= K\mathbb{E}_t^{Q^1} \left\{ \sum_{s=[t]+1}^{\lfloor \tau \rfloor \wedge T} \Pi(Y_{s-1})\mathbb{E}_t^{Q^2} [D(t, s)(R + i_s)] \right\} + K\mathbb{E}_t^{Q^1} [\Pi(Y_T)]\mathbb{E}_t^{Q^2} [D(t, T)] \\ &\quad + K\mathbb{E}_t^{Q^1} \left\{ (\tau - \lfloor \tau \rfloor)\Pi(Y_{\lfloor \tau \rfloor})\mathbb{I}((\tau \leq T))\mathbb{E}_t^{Q^2} [D(t, s)(R + i_\tau)|\tau] \right\}, \end{aligned} \tag{A8}$$

where the pricing measure Q^1 is the distorted probability measure of the catastrophe disaster risk X ; the $\mathbb{E}_t^{Q^1}[\cdot]$ terms usually require simulation to evaluate.

The performance of the financial market is reflected by the interest rate process $\{r_t, t \geq 0\}$ and the Shibor process $\{\ell_t, t \in \mathbb{N}\}$, and these two rates are priced by consummate APT and modeled by a risk-neutral pricing measure Q^2 representing the free arbitrage assumption of investment market. We link the financial market risks with Equation (A8) through

$$D(t, T) = \exp\left(-\int_t^T r_t dt\right), \quad i_t = e^{\ell_t} - 1.$$

The process $\{(r_t, \ell_t), t \geq 0\}$ is modeled with the Vasicek model [29], which is a bivariate correlated Ornstein–Uhlenbeck (OU) process under the risk-neutral measure Q^2 , denoted by

$$\begin{cases} dr_t = a_r(b_r - r_t)dt + \sigma_r dW_{r,t}, \\ d\ell_t = a_\ell(b_\ell - \ell_t)dt + \sigma_\ell dW_{\ell,t}, \end{cases} \tag{A9}$$

where a_r, b_r , and σ_r are the mean reversion rate, long run means, and the volatility, respectively, which are all positive. Moreover, $W_{r,t}$ is standard Brownian motion under Q^2 . Here, the two Brownian motion processes are constantly correlated, i.e., for some $\rho \in (-1, 1)$,

$$dW_{\ell,t}dW_{r,t} = \rho dt, \quad t \geq 0.$$

It follows from [3], we have [29]

$$\mathbb{E}_t^{Q^2}[D(t, s)] = A(t, s)e^{-B(t, s)r_t}, \quad s \geq t \geq 0, \tag{A10}$$

where

$$\begin{cases} A(t, s) = \exp\left\{\frac{(B(t, s) - (s - t))(a_r^2 b_r - \sigma_r^2/2)}{a_r^2} - \frac{\sigma_r^2 B(t, s)^2}{4a_r}\right\}, \\ B(t, s) = \frac{1 - e^{-a_r(s-t)}}{a_r}. \end{cases}$$

And $\mathbb{E}_t^{Q^2}[D(t, s)i_s]$ can be calculated by

$$\begin{aligned} \mathbb{E}_t^{Q^2}[D(t, s)i_s] &= \mathbb{E}_t^{Q^2}[D(t, s)e^{i_s}] - \mathbb{E}_t^{Q^2}[D(t, s)] \\ &= \tilde{A}(t, s) \exp\{-B(t, s)r_t + \tilde{B}(t, s)l_t\} - A(t, s)e^{-B(t, s)r_t}, \quad s \geq t \geq 0, \end{aligned} \tag{A11}$$

where $A(\cdot, \cdot)$ and $B(\cdot, \cdot)$ are defined as above, and $\tilde{A}(\cdot, \cdot)$ and $\tilde{B}(\cdot, \cdot)$ are introduced as below:

$$\begin{cases} \tilde{A}(t, s) = \exp\{-(C_1(t, s) + C_2(t, s))\}, \\ \tilde{B}(t, s) = e^{-a_\ell(s-t)} \end{cases}$$

with

$$\begin{cases} C_1(t, s) = \left(b_r - \frac{\sigma_r^2}{2a_r}\right)(s - t) + \frac{3\sigma_r^2}{4a_r^2} + \frac{\rho\sigma_r\sigma_\ell}{a_\ell(a_\ell - a_r)} + \frac{\sigma_\ell^2}{4a_\ell} + b_\ell - \frac{b_r}{a_r}, \\ C_2(t, s) = \frac{\sigma_r^2}{4a_r^2}e^{-2a_r(s-t)} + \left(\frac{b_r}{a_r} - \frac{\sigma_r^2}{a_r^2}\right)e^{-a_r(s-t)} + \left(\frac{\rho\sigma_r\sigma_\ell}{a_r a_\ell} - b_\ell\right)e^{a_\ell(s-t)} \\ \quad - \frac{\rho\sigma_r\sigma_\ell}{a_r(a_\ell - a_r)}e^{(a_\ell - a_r)(s-t)} - \frac{\sigma_\ell^2}{4a_\ell}e^{2a_\ell(s-t)}. \end{cases}$$

References

1. Chen, J.; Liu, G.; Yang, L.; Shao, Q.; Wang, H. Pricing and simulation for extreme flood catastrophe bonds. *Water Resour. Manag.* **2013**, *27*, 3713–3725. [CrossRef]
2. Kundzewicz, Z.W.; Huang, J.; Pinskiwar, I.; Su, B.; Szwed, M.; Jiang, T. Climate variability and floods in China—A review. *Earth-Sci. Rev.* **2020**, *211*, 103434. [CrossRef]
3. Tang, Q.; Yuan, Z. CAT bond pricing: A product probability measure with POT risk characterization. *ASTIN Bull.* **2019**, *49*, 457–490. [CrossRef]
4. Falk, M.; Hüslér, J.; Reiss, R.D. Extreme Value theory. In *Laws of Small Numbers: Extremes and Rare Events*; Springer: Basel, Switzerland, 2011; pp. 25–101.
5. Cirillo, P.; Taleb, N.N. Tail risk of contagious diseases. *Nat. Phys.* **2020**, *16*, 606–613. [CrossRef]
6. Embrechts, P.; Klüppelberg, C.; Mikosch, T. *Modelling Extremal Events: For insurance and Finance*; Springer Science & Business Media: New York, NY, USA, 2013.
7. Liu, W.; Wu, J.; Tang, R.; Ye, M.; Yang, J. Daily precipitation threshold for rainstorm and flood disaster in the mainland of China: An economic loss perspective. *Sustainability* **2020**, *12*, 407. [CrossRef]
8. Towler, E.; Llewellyn, D.; Prein, A.; Gilleland, E. Extreme-value analysis for the characterization of extremes in Water Resources: A generalized workflow and case study on New Mexico monsoon precipitation. *Weather Clim. Extrem.* **2020**, *29*, 100260. [CrossRef]
9. Aranda, J.A.; García-Bartual, R. Effect of seasonality on the quantiles estimation of maximum floodwater levels in a reservoir and maximum outflows. *Water* **2020**, *12*, 519. [CrossRef]
10. Sun, R.; Gong, Z.; Gao, G.; Shah, A.A. Comparative analysis of multi-criteria decision-making methods for flood disaster risk in the Yangtze river delta. *Int. J. Disaster Risk Reduct.* **2020**, *51*, 101768. [CrossRef]
11. Coles, S.; Heffernan, J.; Tawn, J. Dependence measures for extreme value analyses. *Extremes* **1999**, *2*, 339–365. [CrossRef]
12. Lin, H.; Zhang, Z. Extreme co-movements between infectious disease events and crude oil futures prices: From extreme value analysis perspective. *Energy Econ.* **2022**, *110*, 106054. [CrossRef]
13. Evgenidis, A.; Tsagkanos, A.; Siriopoulos, C. Towards an asymmetric long-run equilibrium between economic uncertainty and the yield spread. A multi-economy view. *Res. Int. Bus. Financ.* **2017**, *39*, 267–279. [CrossRef]
14. Surminski, S.; Dorta, D. Flood insurance schemes and climate adaptation in developing countries. *Int. J. Disaster Risk Reduct.* **2014**, *7*, 154–164. [CrossRef]

15. Loretan, M.; Philips, P.C.B. Testing the covariance stationarity of heavy tailed time series: An overview of the theory with applications to several financial datasets. *J. R. Stat. Soc.* **1994**, *1*, 211–248. [[CrossRef](#)]
16. Coles, S. *An Introduction to Statistical Modeling of Extreme Values*; Springer Series in Statistics; Springer: London, UK, 2001.
17. Scarrott, C.; MacDonald, A. A review of extreme value threshold estimation and uncertainty quantification. *Rev. Stat. J.* **2021**, *10*, 33–60.
18. Zhao, Y.; Gong, Z.; Wang, W.; Luo, K. The comprehensive risk evaluation on rainstorm and flood disaster losses in China mainland from 2004 to 2009: Based on the triangular grey correlation theory. *Nat. Hazards* **2014**, *71*, 1001–1016. [[CrossRef](#)]
19. Wang, S.S. A class of distortion operators for pricing financial and insurance risks. *J. Risk Insur.* **2000**, *67*, 15–36. [[CrossRef](#)]
20. Shao, J.; Pantelous, A.; Papaioannou, A.D. Catastrophe risk bonds with applications to earthquakes. *Eur. Actuar. J.* **2015**, *5*, 113–138. [[CrossRef](#)]
21. Cui, P.; Peng, J.; Shi, P.; Tang, H.; Ouyang, C.; Zou, Q.; Liu, Q.; Lei, Y. Scientific challenges of research on natural hazards and disaster risk. *Geogr. Sustain.* **2021**, *2*, 216–223. [[CrossRef](#)]
22. Ho, C.T. Measuring bank operations performance: An approach based on grey relation analysis. *J. Oper. Res. Soc.* **2006**, *57*, 337–349. [[CrossRef](#)]
23. Alston, A. A Bayesian Spatial Analysis of Extreme Precipitation. Ph.D. Thesis, North Carolina State University, Raleigh, NC, USA, 2011.
24. Koh, J.; Pimont, F.; Dupuy, J.L.; Opitz, T. Spatiotemporal wildfire modeling through point processes with moderate and extreme marks. *arXiv* **2021**, arXiv:2105.08004.
25. Ibrahim, R.A.; Napitupulu, H. Multiple-trigger catastrophe bond pricing model and its simulation using numerical methods. *Mathematics* **2022**, *10*, 1363. [[CrossRef](#)]
26. Wei, L.; Liu, L.; Hou, J. Pricing hybrid-triggered catastrophe bonds based on copula-EVT model. *Quant. Financ. Econ.* **2022**, *6*, 223–243. [[CrossRef](#)]
27. Gilleland, E.; Katz, R.W. Extremes 2.0: An extreme value analysis package in R. *J. Stat. Softw.* **2016**, *72*, 1–39. [[CrossRef](#)]
28. Wang, R.; Wei, Y. Characterizing optimal allocations in quantile-based risk sharing. *Insur. Math. Econ.* **2020**, *93*, 288–300. [[CrossRef](#)]
29. Mamon, R.S. Three ways to solve for bond prices in the Vasicek model. *J. Appl. Math. Decis. Sci.* **2004**, *8*, 1–14. [[CrossRef](#)]

Disclaimer/Publisher’s Note: The statements, opinions and data contained in all publications are solely those of the individual author(s) and contributor(s) and not of MDPI and/or the editor(s). MDPI and/or the editor(s) disclaim responsibility for any injury to people or property resulting from any ideas, methods, instructions or products referred to in the content.